EARTH SCIENCES
RESEARCH JOURNAL

Earth Sci. Res. J. Vol. 23, No. 2 (June, 2019): 133-146

UNIVERSIDAD NACIONAL DE COLOMBIA

GEOCHEMISTRY

Mineralogical features and petrogenetic significance of the clinopyroxene and hornblende of the Wuhaolai mafic complex in northern North China Craton, Inner Mongolia

Wang Chen[1]*, Liu Jianchao1, Zhang Haidong[1, 2], Ge Jiakun1, Xi Zhixuan[1], Wang Haoran[1]
[1]School of Earth Science and Resources. Chang'an University, China.
[2]Department of Geology, Northwest University, China
* Corresponding author: chenwchd@163.com

ABSTRACT

The Wuhaolai mafic complex is located in the north margin of the North China Craton (NCC), Inner Mongolia. To discuss the mineralogical features, magma evolution process, and tectonic setting of the complex, we analyzed the geochemical compositions of clinopyroxene and hornblende using an electron probe. The results revealed that the parental magma of this complex belonged to the intraplate alkaline basalt series. The normal zoning texture and the relation between Mg# and FeO, Al2O3, CaO, Na2O, SiO2 and Cr2O3 suggested that the clinopyroxenes of pyroxenite and gabbro crystallized from the same parental magma. The similar CaO content of clinopyroxenes indicated that the parental magma of the Wuhaolai complex may have suffered crustal contamination. Furthermore, the characteristics of hornblende demonstrated that the magma source was modified by fluids derived from subducted slab. Based on the value of Kdcpx (0.23–0.27), the equilibrium melt with clinopyroxene exhibited a relatively low Mg# (43–53), indicating that the parental magma was derived from the lithospheric mantle and underwent crystal fractionation. The gabbro crystallization temperature and pressure was found to be lower than that of pyroxenite, indicating that gabbro was formed at a lower depth than that of pyroxenite. Combining the tectonic setting discrimination diagram of clinopyroxene with the results of previous studies on the late Paleozoic intrusions near the research area, we proposed that the Wuhaolai complex was formed in an intraplate environment. The magma source was modified by fluids derived from the subducted slab during the subduction of the Paleo-Asian Ocean (PAO). After the PAO closure, the parental magma of the Wuhaolai complex was produced by the partial melting of the enriched lithospheric mantle

Keywords: Wuhaolai mafic complex; genetic mineralogy; magmatic evolution; tectonic significance; margin of the North China Craton.

Características mineralógicas y significado petrogenético del clinopiroxeno y la hornblenda del complejo máfico de Wuhaolai en el Cratón del Norte de China, Mongolia Interior

RESUMEN

El complejo máfico de Wuhaolai está ubicado en el margen norte del Cratón del Norte de China (NCC), Mongolia Interior. Para analizar las características mineralógicas, el proceso de evolución del magma y el ajuste tectónico del complejo, analizamos las composiciones geoquímicas de clinopiroxeno y hornblenda utilizando una microsonda de electrones. Los resultados revelaron que el magma parental de este complejo pertenecía a la serie de basalto alcalino intraplaca. La textura normal de zonificación y la relación entre Mg # y FeO, Al2O3, CaO, Na2O, SiO2 y Cr2O3 sugirieron que los clinopiroxenos de piroxenita y gabbro se cristalizaron del mismo magma parental. El contenido similar de CaO de los clinopiroxenos indica que el magma parental del complejo Wuhaolai puede haber sufrido contaminación de la corteza. Además, las características de la hornblenda demostraron que la fuente de magma fue modificada por fluidos derivados de la losa subducida. Sobre la base del valor de Kdcpx (0.23–0.27), la masa fundida en equilibrio con clinopiroxeno exhibió un número de Mg relativamente bajo (43–53), lo que indica que el magma parental se derivó del manto litosférico y se sometió a un fraccionamiento de cristales. Se encontró que la temperatura y la presión de cristalización de gabbro eran más bajas que la de piroxenita, lo que indica que el gabro se formó a una profundidad más baja que la piroxenita. Combinando el diagrama de discriminación del ajuste tectónico del clinopiroxeno con los resultados de estudios previos sobre las últimas intrusiones del Paleozoico cerca del área de investigación, proponemos que el complejo Wuhaolai se forma en un entorno intraplaca. La fuente de magma fue modificada por fluidos derivados de la losa subducida durante la subducción del Océano Paleoasiático (PAO). Después del cierre de la PAO, el magma parental del complejo Wuhaolai se produjo mediante la fusión parcial del manto litosférico enriquecido

Palabras clave: complejo máfico de Wuhaolai; mineralogía genética; evolución magmática; significación tectónica; margen del Cratón China del Norte.

Record
Manuscript received: 14/07/2017
Accepted for publication: 30/11/2018

How to cite item
Chen, W., Jianchao, L., Haidong, Z., Jiakun, G., Zhixuan, X., Haoran, W. (2019). Mineralogical features and petrogenetic significance of the clinopyroxene and hornblende of the Wuhaolai mafic complex in northern North China Craton, Inner Mongolia. *Earth Sciences Research Journal*, 23(2), 133-146. DOI: https://doi.org/10.15446/esrj.v23n2.66316

Introduction

As one of the oldest cratons in the world, the formation of the North China Craton (NCC) can traced back to approximately 1.8 Ga (Zhao et al., 2001; Wilde et al., 2002). The interior of NCC is generally believed to have been stable from the Mesoproterozoic to Triassic (Robinson et al., 1999; Wilde et al., 2002; Kusky et al., 2007). However, the southward subduction of the Paleo-Asia Ocean (PAO) caused dramatic tectono-magmatic activities during the late Paleozoic in the northern NCC (Davis et al., 2001; Xiao et al., 2003; Zhang et al., 2007a; Ying et al., 2011; Menzies et al., 1993; Wilde et al., 2003; Yang et al., 2008; Wu et al., 2008). Moreover, large numbers of the late Paleozoic–early Mesozoic plutonic rocks are distributed along the northern NCC (Pan et al., 1996; Zhang et al., 2007b).

Similar to the circum-Pacific orogenic belt, the northern NCC margin comprises an island arc, a ridge, an oceanic island, a seamount, an oceanic basin, an accretionary wedge, and a micro plate, forming a complex tectonic framework (Windley et al., 2007). In addition, there still is a great controversy on the PAO closure time in terms of the spatio-temporal distribution of the ophiolites, multi-stage tectonic deformations, and magmatic activities in the northern NCC margin (Zhao et al., 2011). According to the prevailing hypothesis, the PAO closed in the Ordovician–Silurian (Han et al., 1997; Kheraskova et al., 2003), the Devonian–Late Carboniferous (Shi et al., 2013; Zhao et al., 2013), or the Permian–Late Triassic (Jian et al., 2010; Li et al., 2014a; Li et al., 2014b).

In this research, we study the Wuhaolai mafic complex that is located in Xinhure, Inner Mongolia. The Wuhaolai mafic complex is located in the middle segment of the northern NCC, south of the Central Asia Orogenic Belt (CAOB; Fig. 1a). The complex is part of a mafic–ultramafic belt, which is distributed among the Wulatezhongqi, Damaoqi, and Bayan Obo areas (Fig. 1b) (Cao et al., 2002; Zhao, 2008). Studies on this mafic belt indicated that the Huheengeer pluton (242–287 Ma) was formed in an active continental margin (Zhao et al., 2008). Nevertheless, the Beiqigetao pluton (269 Ma ± 8 Ma) and the Tugurige pluton (273.5 Ma ± 1.3 Ma) formed in a post-collisional extension setting (Zhao et al., 2011; Wang et al., 2016). However, previous research mainly focused on the petrology and whole-rock geochemistry, but the mineralogical analyses were not enough documented. In this research, we focused on the characteristics of the rock-forming minerals (e.g., clinopyroxene and hornblende) using electron microprobe analytical data to investigate the evolution of the parental magma and discuss the tectonic setting in the study area.

Geological background and petrography

The Wuhaolai mafic complex is located near the Wulatezhongqi area, Inner Mongolia, China. The Solonker ophiolite belt, which is considered as a suture zone between the NCC and the Siberian Craton (SC), is situated in the northern part of this complex (Fig. 1b) (Wu et al., 1998; Xiao et al. 2003; Li et al., 2006; Windley et al. 2007). The late Archean crystalline basement of this area is represented by the East Wufuzi formation, which comprises actinolite–biotite schist, biotite–plagioclase gneiss, and biotite–monzonitic gneiss (Fig. 2a). In addition, the Bayan Obo Group, which comprises conglomeratic sandstone, sandy slate, slate, and sandy limestone, lies uncomfortably over the crystalline basement (Fig. 2b).

The Wuhaolai mafic complex is a N–W striking stock, comprising from the center to the rim pyroxenite, gabbro and diorite units respectively (Fig. 2b). In this research, two pyroxenite samples, two gabbro samples and one diorite sample were selected to study the petrography section. Pyroxenite displays medium-coarse grain texture and massive structure with a black-green color (Figs. 3a and 3b). Furthermore, pyroxenite mainly contains subhedral, zonal clinopyroxene (80 vol.%; 0.2–1 mm in length), subhedral hornblende (10 vol.%,; 0.5-1 mm in length), subhedral plagioclase (5 vol.% ; ~0.5 mm in length) and rare magnetite (5 vol.%). Gabbro (Fig. 3c and 3d) was grayish white, with a coarse medium-grained texture and massive structure. It contains 40 vol.% of anhedral–granular clinopyroxene, 40 vol.% of coarse -grained subhedral hornblende, and 20 vol.% of subhedral, zonal plagioclase with characteristic polysynthetic twins. Diorite (Figs. 3e and 3f) displays a coarse medium-grained texture and massive structure. It mainly comprises zonal, coarse medium-grained subhedral plagioclase (45 vol.%) and coarse medium-grained subhedral hornblende (30 vol.%), fine grained quarte (15%) and biotite (10 vol.%). From Figs. 3b and 3d, the subhedral hornblende cuts across the clinopyroxene, indicating that clinopyroxene crystallized earlier than hornblende.

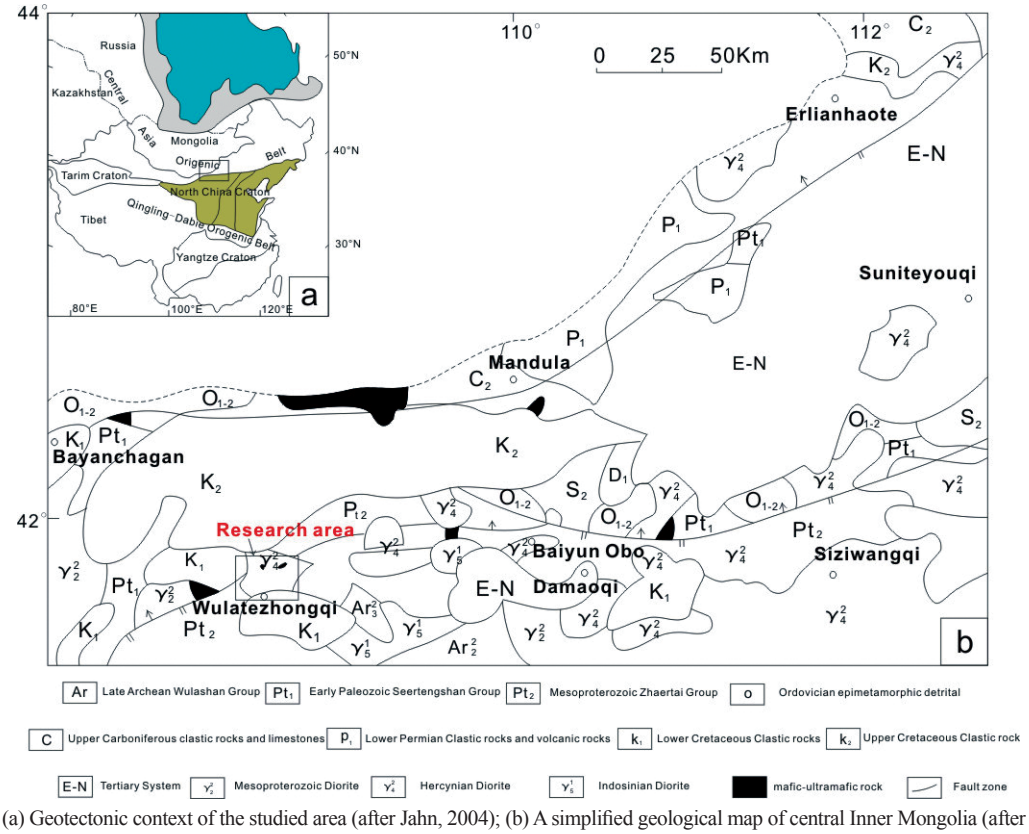

Figure 1. (a) Geotectonic context of the studied area (after Jahn, 2004); (b) A simplified geological map of central Inner Mongolia (after Cao et al., 2002).

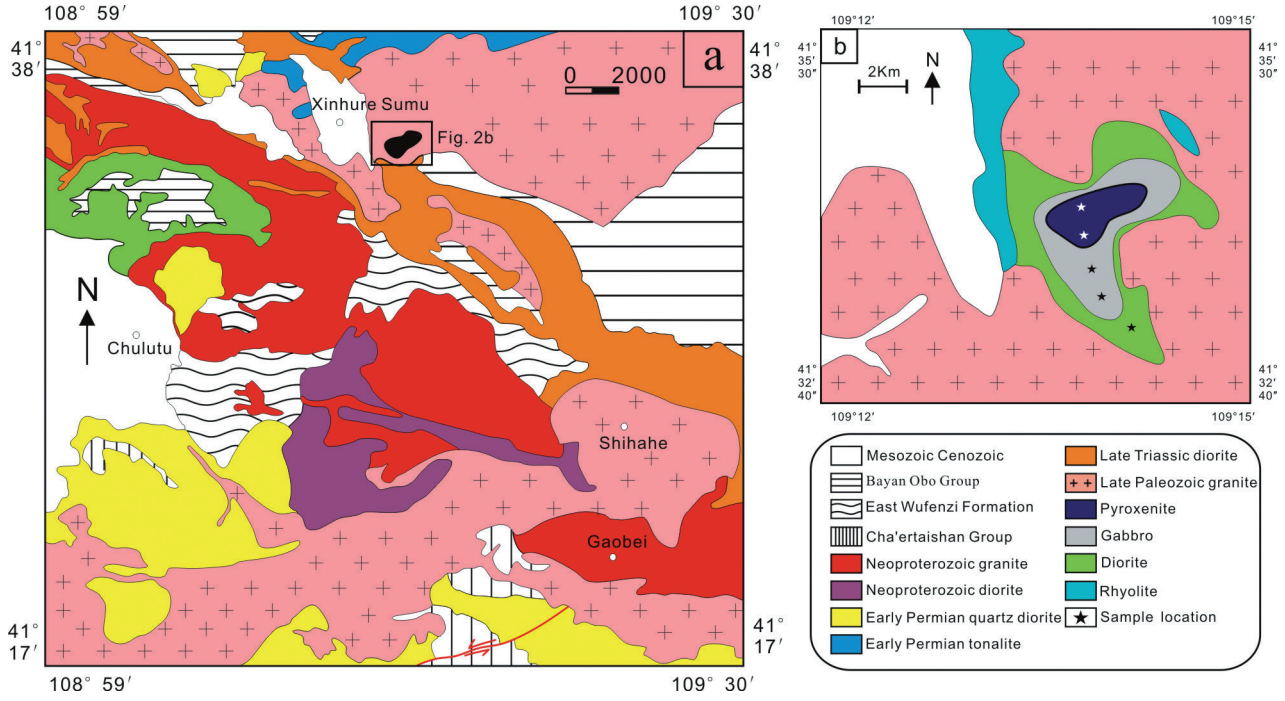

Figure 2. (a) Geological map of the Xinhure area (after Hao et al., 2016); (b) Geological map of the Wuhaolai mafic complex (after IMBGMR, 1991).

Analytical methods and results

The microanalysis of clinopyroxenes and hornblendes crystals in the studied samples of pyroxenite, gabbro and diorite from the Wuhaolai mafic complex was conducted at the Laboratory of Mineralization and Dynamics, Chang'an University. A JEOL JXA-8200 electron microscope with ZAF matrix correction. The analysis was used with an accelerating potential of 15 kV, a sample current of 1×10^{-8} A, and a spot diameter of 0.5 μm, and counting time of 10 s. The standards of Na, Si, Fe, K, Al, Mn, Ca, Mg, and Ti were natural minerals, and the standard for Cr was synthetic oxides. GeoKit software (Lu, 2004) was used to calculate the geochemical parameters of clinopyroxenes and hornblende. The results are shown in Tables 1 and 2.

Based on the pyroxene classification standards (Morimoto et al., 1988), the clinopyroxene grains from the Wuhaolai mafic complex belong to the Ca–Mg–Fe species. In the Wo–En–Fs diagram (Fig.4a), clinopyroxene grains from pyroxenite are plotted into the diopside compositional field (Wo = 48.24–49.52, En = 39.06–39.93, Fs = 10.17–11.29), which shows a small variation in the composition, with 51.79 wt.%–52.82 wt.% SiO_2, 13.91 wt.%–14.43 wt.% MgO, 24.01 wt.%–24.69 wt.% CaO, 5.52 wt.%–6.48 wt.% FeO, 0.001 wt.%–0.132 wt.% TiO_2, 0.42 wt.%–1.21 wt.% Al_2O_3, 0.23 wt.%–0.42 wt.% Na_2O, 0.01 wt.%–0.086 wt.% Cr_2O_3, and Mg# (=100 Mg/(Mg + Fe_{total})) in the range 79–82. Additionally, clinopyroxene grains from gabbro also plot into the diopside compositional field (Wo = 47.43–49.42, En = 38.72–40.1, Fs = 10.34–11.21) with the geochemical characteristics of 51.22 wt.%–52.97 wt.% SiO_2, 13.59 wt.%–14.49 wt.% MgO, 23.75 wt.%–24.32 wt.% CaO, 5.68 wt.%–6.31 wt.% FeO, 0.1 wt.%–0.2 wt.% TiO_2, 0.88 wt.%–1.54 wt.%Al_2O_3, 0.32 wt.%–0.48 wt.% Na_2O, 0.03 wt.%–0.11 wt.% Cr_2O_3, and Mg# in the range 79–81.

The cations of hornblende from pyroxenite are characterized by Ca_B = 1.90–1.97 and $(Na + K)_A$ = 0.28–0.61, and the cations of hornblende from gabbroare characterized by Ca_B = 1.77–1.93 and $(Na + K)_A$ = 0.45–0.54. The hornblende grains from the complex belong to calcic hornblende. Based on the classification scheme of calcic hornblende (Leake et al., 1997), the hornblendes from pyroxenite and gabbro are edenite, which have relatively lower SiO_2 (43.61 wt.%–48.97 wt.%), MgO (12.22 wt.%–15.13 wt.%), CaO (12.15 wt.%–12.55 wt.%), and Si/(Si + Ti + Al) in the range 0.28–0.68 as well as higher TiO_2 (0.59 wt.%–1.67 wt.%), Al_2O_3 (6.24 wt.%–11.30 wt.%), and Na_2O (0.81 wt.%–1.48 wt.%). The hornblendes from diorite are magnesio-hastingsites with relatively higher SiO_2 (46.75 wt.%–48.3 wt.%), MgO (14.06 wt.%–14.93 wt.%), CaO (12.23 wt.%–12.86 wt.%), and Si/(Si + Ti + Al) in the range 0.72–0.75 as well as lower TiO_2 (0.86 wt.%–1.03 wt.%), Al_2O_3 (8.21 wt.%–8.60 wt.%), and Na_2O (1.01 wt.%–1.28 wt.%) (Fig. 4b).

Discussion

Mineral genesis and magmatic evolution

In the Ti–(Ca + Na) diagram (Fig. 5), the clinopyroxenes from the Wuhaolai mafic complex belong to the alkaline series. Compared with the characteristics of arc basalt (ArcB) and ocean island basalt (OIB) (Condie K.C., 1982), the clinopyroxenes from the Wuhaolai mafic complex have lower Mg#, CaO, SiO_2, and Cr_2O_3 contents and higher Al_2O_3 and Na_2O contents. Additionally, the Mg# of clinopyroxene has a negative correlation with FeO and Al_2O_3 and a positive correlation with Na_2O (Fig. 6a-d). Furthermore, all analyzed clinopyroxene grains plot into or near the continental alkaline basalt (CAB) area (Figs. 6e-h), indicating that the parental magma of this mafic complex has chemical characteristics consistent with the intra-plate alkaline series. The geochemical profile of the clinopyroxene grains (Figs. 7a and 7b) reflects a normal zonal feature with a higher Mg# and lower Al_2O_3, Na_2O, and TiO_2 contents in the core than at the rims (Zhao et al., 2011). It is interpreted that clinopyroxenes in pyroxenite and gabbro are crystallized from the same magma (Yu et al., 2011; Zhao et al., 2011). With the crystallization of clinopyroxene, Mg first entered into the crystalline phase, followed by Ca and Al, and finally was Na and K (Bowen, 1928). Thus, the crystallization of clinopyroxene may led to the magma rich in the Si, Na and K and depleted in the Mg, Ca and Al. Thus, the decreasing MgO, FeO and Al_2O_3 contents of clinopyroxenes from pyroxenite to gabbro were conforming to the magma evolution process. However, compared with the normal crystallization evolution of magma, the CaO content of gabbro was higher than the pyroxenite. Since crustal contamination depends on the compositions of the surrounding rocks (Su et al., 2009; Liu et al., 2012), the crystalline basement in the study area, which comprises biotite schist, limestone, and other rocks, contains a sufficient amount of Ca. Previous research shows that the parental magma of ankaramite in South Margin of the Altay Mountains has not suffered the crustal contamination (Su et al., 2008). The clinopuroxene CaO content of the ankaramite was 18.5%-22.07%, which was obviously lower than the Wuhaolao complex. Thus, the parental magma of the Wuhaolai mafic complex may have suffered the crustal contamination during its evolution. Previous research has shown

Table 1. Electron-microprobe compositions of Clinopyroxene from the Wuhaolai complex

Samples	**HS-1**	**HS-2**	**HS-3**	**HS-4**	**HS-5**	**HS-6**	**HS-7**	**HS-8**	**HC-1**	**HC-2**	**HC-3**	**HC-4**	**HC-5**	**HC-6**	**HC-7**	**HC-8**
	pyroxenite								**gabbro**							
SiO_2	51.80	52.90	51.80	52.97	52.53	52.93	52.17	52.11	52.17	52.67	52.82	52.54	52.22	52.25	51.80	52.27
TiO_2	0.13	0.13	0.13	0.10	0.13	0.16	0.19	0.20	0.04	0.13	0.08	0.00	0.09	0.11	0.12	0.04
Al_2O_3	0.88	0.95	0.88	0.93	0.99	1.02	1.01	1.05	0.64	0.99	0.81	0.42	0.98	0.84	1.22	0.77
Cr_2O_3	0.05	0.08	0.05	0.10	0.03	0.11	0.03	0.08	0.00	0.09	0.00	0.00	0.01	0.03	0.08	0.00
Fe_2O_3	0.70	0.66	0.70	0.65	0.67	0.67	0.70	0.63	0.72	0.66	0.67	0.61	0.67	0.66	0.65	0.69
FeO	6.29	6.26	6.29	6.27	6.32	6.06	6.31	5.98	6.48	5.92	5.99	5.52	6.07	5.97	5.84	6.21
MnO	0.19	0.24	0.19	0.33	0.23	0.28	0.27	0.24	0.10	0.24	0.16	0.42	0.12	0.14	0.17	0.29
MgO	14.02	14.50	14.02	14.11	14.18	14.18	13.59	13.69	14.09	14.09	14.29	14.10	14.24	14.44	13.95	13.91
CaO	24.10	23.86	24.10	24.11	23.75	24.32	24.01	24.21	24.29	24.40	24.06	24.69	24.06	24.26	24.37	24.01
Na_2O	0.35	0.41	0.35	0.32	0.36	0.32	0.37	0.37	0.23	0.33	0.36	0.26	0.32	0.40	0.42	0.25
K_2O	0.01	0.00	0.01	0.00	0.00	0.00	0.01	0.00	0.00	0.00	0.00	0.00	0.00	0.00	0.00	0.00
Si	1.96	1.97	1.96	1.97	1.98	1.96	1.97	1.96	1.97	1.97	1.97	1.98	1.96	1.96	1.95	1.97
Al(iv)	0.00	0.03	0.00	0.03	0.02	0.04	0.03	0.04	0.00	0.03	0.03	0.00	0.04	0.00	0.05	0.03
Al(vi)	0.00	0.01	0.00	0.02	0.02	0.01	0.02	0.03	0.00	0.01	0.01	0.00	0.01	0.00	0.01	0.01
Ti	0.00	0.00	0.00	0.00	0.00	0.00	0.01	0.01	0.00	0.00	0.00	0.00	0.00	0.00	0.00	0.00
Cr	0.00	0.00	0.00	0.00	0.00	0.00	0.00	0.00	0.00 .	0.00	.0.00	0.00 .	0.00	0.00	0.00	0.00
Fe^{3+}	0.02	0.02	0.02	0.02	0.02	0.02	0.02	0.02	0.02	0.02	0.02	0.02	0.02	0.02	0.02	0.02
Fe^{2+}	0.20	0.19	0.20	0.18	0.19	0.19	0.20	0.18	0.20	0.18	0.19	0.17	0.19	0.19	0.18	0.20
Mn	0.01	0.01	0.01	0.01	0.01	0.01	0.00	0.01	0.00	0.01	0.01	0.01	0.00	0.00	0.01	0.01
Mg	0.79	0.80	0.79	0.78	0.77	0.78	0.76	0.76	0.79	0.78	0.80	0.79	0.80	0.81	0.78	0.78
Ca	0.98	0.95	0.98	0.96	0.96	0.97	0.96	0.97	0.98	0.98	0.96	1.00	0.97	0.98	0.98	0.97
Na	0.03	0.03	0.03	0.02	0.03	0.02	0.03	0.03	0.02	0.02	0.03	0.02	0.02	0.03	0.03	0.02
K	0.00	0.00	0.00	0.00	0.00	0.00	0.00	0.00	0.00	0.00	0.00	0.00	0.00	0.00	0.00	0.00
Wo	48.40	48.40	48.63	48.59	48.53	48.58	48.68	49.42	48.64	48.92	48.64	48.92	48.34	48.24	49.04	48.63
En	39.19	39.19	38.72	39.56	39.19	39.42	38.73	38.87	39.24	39.32	39.24	39.32	39.81	39.93	39.06	39.19
Fs	11.14	11.14	11.02	10.67	10.96	10.85	11.21	10.34	11.29	10.56	11.29	10.56	10.67	10.41	10.37	11.27
Ac	1.28	1.28	1.63	1.18	1.33	1.16	1.38	1.37	0.83	1.20	0.83	1.20	1.17	1.42	1.54	0.90

Table 2. Electron-microprobe compositions of hornblende from the Wuhaolai complex

Samples	HS-1	HS-2	HS-3	HS-4	HS-5	HS-6	HS-7	HS-8	HS-9	HS-10	HS-11	HS-12
	pyroxenite											
SiO_2	45.03	43.61	44.81	46.77	47.98	48.98	48.67	48.26	48.56	47.37	45.12	44.67
TiO_2	1.15	1.68	1.18	0.89	0.60	0.71	0.63	0.69	0.66	0.84	1.16	1.29
Al_2O_3	9.55	11.30	9.63	8.30	6.57	6.42	6.37	6.56	6.25	7.53	8.96	9.56
FeO	12.94	12.82	12.48	11.65	11.47	11.47	11.55	11.30	11.00	12.29	12.92	13.03
MnO	0.22	0.12	0.07	0.13	0.19	0.10	0.20	0.14	0.26	0.24	0.22	0.25
MgO	13.56	12.22	13.17	14.21	14.84	15.13	14.83	14.80	14.76	14.17	13.25	12.75
CaO	12.29	12.15	12.48	12.55	12.53	12.42	12.43	12.34	12.47	12.55	12.35	12.33
Na_2O	1.20	1.48	1.26	0.95	0.87	0.89	0.81	0.93	0.96	0.85	1.17	1.32
K_2O	0.59	0.99	0.81	0.43	0.31	0.26	0.29	0.30	0.26	0.38	0.56	0.57
Si	6.70	6.52	6.71	6.93	7.13	7.18	7.19	7.16	7.20	7.01	6.77	6.71
Al^{IV}	1.30	1.48	1.29	1.07	0.87	0.82	0.81	0.84	0.80	0.99	1.23	1.29
Al^{VI}	0.37	0.51	0.41	0.38	0.28	0.29	0.29	0.30	0.30	0.32	0.35	0.40
Ti	0.13	0.19	0.13	0.10	0.07	0.08	0.07	0.08	0.07	0.09	0.13	0.15
Fe^{3+}	0.44	0.39	0.43	0.58	0.62	0.66	0.67	0.65	0.66	0.60	0.47	0.45
Fe^{2+}	1.17	1.21	1.13	0.87	0.81	0.75	0.76	0.76	0.70	0.92	1.15	1.18
Mn	0.03	0.02	0.01	0.02	0.02	0.01	0.03	0.02	0.03	0.03	0.03	0.03
Mg	3.01	2.72	2.94	3.14	3.29	3.31	3.26	3.27	3.26	3.13	2.96	2.86
Ca	1.96	1.95	2.00	1.99	1.99	1.95	1.97	1.96	1.98	1.99	1.99	1.98
Na	0.35	0.43	0.36	0.27	0.25	0.25	0.23	0.27	0.28	0.24	0.34	0.38
K	0.11	0.19	0.16	0.08	0.06	0.05	0.05	0.06	0.05	0.07	0.11	0.11
Total cations	15.56	15.61	15.57	15.42	15.38	15.34	15.33	15.35	15.34	15.40	15.53	15.55
OH^-	0.00	0.00	0.00	0.00	0.00	0.00	0.00	0.00	0.00	0.00	0.00	0.00
F	0.00	0.00	0.00	0.00	0.00	0.00	0.00	0.00	0.00	0.00	0.00	0.00
Cl	0.00	0.00	0.00	0.00	0.00	0.00	0.00	0.00	0.00	0.00	0.00	0.00
Si_T*	6.70	6.52	6.71	6.93	7.13	7.18	7.19	7.16	7.20	7.01	6.77	6.71
Al_T	1.30	1.48	1.29	1.07	0.87	0.82	0.81	0.84	0.80	0.99	1.23	1.29
Al_C	0.37	0.51	0.41	0.38	0.28	0.29	0.29	0.30	0.30	0.32	0.35	0.40
$Fe^{3+}{}_C$	0.44	0.39	0.43	0.58	0.62	0.66	0.67	0.65	0.66	0.60	0.47	0.45
Ti_C	0.13	0.19	0.13	0.10	0.07	0.08	0.07	0.08	0.07	0.09	0.13	0.15
Mg_C	3.01	2.72	2.94	3.14	3.29	3.31	3.26	3.27	3.26	3.13	2.96	2.86
$Fe^{2+}{}_C$	1.05	1.18	1.09	0.81	0.75	0.67	0.70	0.70	0.70	0.86	1.08	1.15
Mn_C	0.00	0.00	0.00	0.00	0.00	0.00	0.00	0.00	0.00	0.00	0.00	0.00
$Fe^{2+}{}_B$	0.12	0.03	0.04	0.06	0.06	0.08	0.06	0.05	0.00	0.06	0.07	0.04
Mn_B	0.03	0.02	0.01	0.02	0.02	0.01	0.03	0.02	0.03	0.03	0.03	0.03
Ca_B	1.85	1.95	1.95	1.92	1.92	1.91	1.92	1.93	1.97	1.91	1.90	1.93
Na_B	0.00	0.01	0.00	0.00	0.00	0.00	0.00	0.00	0.00	0.00	0.00	0.00
Ca_A	0.11	0.00	0.05	0.07	0.07	0.04	0.05	0.03	0.01	0.08	0.08	0.05
Na_A	0.35	0.42	0.36	0.27	0.25	0.25	0.23	0.27	0.28	0.24	0.34	0.38
K_A	0.11	0.19	0.16	0.08	0.06	0.05	0.05	0.06	0.05	0.07	0.11	0.11

Continued Table 2. Electron-microprobe compositions of hornblende from the Wuhaolai complex

Samples	HC-1	HC-2	HC-3	HC-4	HC-5	HC-6	SC-1	SC-2	SC-3	SC-4	SC-5	SC-6	SC-7	SC-8	SC-9	SC-10	SC-11	SC-12
	gabbro						diorite											
SiO_2	47.00	47.64	47.70	48.31	47.44	46.75	43.17	43.32	43.24	43.71	44.12	44.08	44.05	43.76	43.70	43.40	43.46	42.95
TiO_2	0.96	0.92	0.86	0.90	0.96	1.03	0.82	1.10	1.11	1.10	0.92	0.98	0.99	1.12	1.06	0.78	0.99	1.08
Al_2O_3	8.59	8.36	8.21	8.31	8.41	8.60	10.34	9.85	9.42	9.28	10.08	9.38	9.40	8.52	9.88	10.12	9.60	9.93
FeO	11.16	10.16	10.51	11.23	11.34	11.82	18.57	19.33	18.37	18.08	18.08	18.21	18.17	16.49	18.92	17.28	18.42	18.22
MnO	0.19	0.26	0.21	0.24	0.17	0.22	0.25	0.22	0.37	0.37	0.41	0.38	0.41	0.38	0.38	0.28	0.33	0.21
MgO	14.16	14.52	14.90	14.06	14.93	14.30	9.52	9.66	9.86	10.21	10.11	10.10	10.10	10.06	9.86	9.37	10.18	9.87
CaO	12.45	12.31	12.59	12.86	12.23	12.34	11.69	11.54	11.49	11.65	11.77	11.67	11.48	11.71	11.70	11.85	11.67	11.69
Na_2O	1.11	1.10	1.01	1.12	1.29	1.28	1.17	1.42	1.26	1.36	1.24	1.24	1.24	1.11	1.29	1.15	1.20	1.31
K_2O	0.48	0.45	0.44	0.45	0.45	0.56	0.52	0.60	0.56	0.59	0.55	0.56	0.54	0.57	0.57	0.57	0.50	0.65
Si	6.93	7.01	6.98	7.02	6.92	6.87	6.63	6.62	6.67	6.69	6.67	6.72	6.72	6.83	6.64	6.71	6.65	6.61
Al^{IV}	1.07	0.99	1.02	0.98	1.08	1.13	1.37	1.38	1.33	1.31	1.33	1.28	1.28	1.17	1.36	1.29	1.35	1.39
Al^{VI}	0.42	0.46	0.40	0.44	0.36	0.36	0.50	0.39	0.38	0.36	0.47	0.40	0.42	0.40	0.41	0.56	0.39	0.41
Ti	0.11	0.10	0.10	0.10	0.11	0.11	0.09	0.13	0.13	0.13	0.11	0.11	0.11	0.13	0.12	0.09	0.11	0.12
Fe^{3+}	0.58	0.64	0.60	0.63	0.52	0.50	0.44	0.36	0.41	0.39	0.44	0.44	0.45	0.52	0.40	0.50	0.41	0.38
Fe^{2+}	0.80	0.61	0.69	0.74	0.86	0.96	1.95	2.11	1.96	1.92	1.85	1.88	1.87	1.63	2.01	1.74	1.95	1.97
Mn	0.02	0.03	0.03	0.03	0.02	0.03	0.03	0.03	0.05	0.05	0.05	0.05	0.05	0.05	0.05	0.04	0.04	0.03
Mg	3.11	3.18	3.25	3.04	3.24	3.13	2.18	2.20	2.27	2.33	2.28	2.29	2.30	2.34	2.23	2.16	2.32	2.26
Ca	1.97	1.94	1.97	2.00	1.91	1.94	1.92	1.89	1.90	1.91	1.91	1.91	1.88	1.96	1.90	1.96	1.92	1.93
Na	0.32	0.31	0.29	0.32	0.36	0.36	0.35	0.42	0.38	0.40	0.36	0.37	0.37	0.34	0.38	0.35	0.35	0.39
K	0.09	0.08	0.08	0.08	0.08	0.11	0.10	0.12	0.11	0.11	0.11	0.11	0.11	0.11	0.11	0.11	0.10	0.13
Total cations	15.42	15.36	15.40	15.37	15.48	15.50	15.56	15.64	15.59	15.61	15.56	15.56	15.55	15.48	15.60	15.50	15.59	15.62
OH^-	0.00	0.00	0.00	0.00	0.00	0.00	0.00	0.00	0.00	0.00	0.00	0.00	0.00	0.00	0.00	0.00	0.00	0.00
F	0.00	0.00	0.00	0.00	0.00	0.00	0.00	0.00	0.00	0.00	0.00	0.00	0.00	0.00	0.00	0.00	0.00	0.00
Cl	0.00	0.00	0.00	0.00	0.00	0.00	0.00	0.00	0.00	0.00	0.00	0.00	0.00	0.00	0.00	0.00	0.00	0.00
Si_T*	6.93	7.01	6.98	7.02	6.92	6.87	6.63	6.62	6.67	6.69	6.67	6.72	6.72	6.83	6.64	6.71	6.65	6.61
Al_T	1.07	0.99	1.02	0.98	1.08	1.13	1.37	1.38	1.33	1.31	1.33	1.28	1.28	1.17	1.36	1.29	1.35	1.39
Al_C	0.42	0.46	0.40	0.44	0.36	0.36	0.50	0.39	0.38	0.36	0.47	0.40	0.42	0.40	0.41	0.56	0.39	0.41
Fe^{3+}_C	0.58	0.64	0.60	0.63	0.52	0.50	0.44	0.36	0.41	0.39	0.44	0.44	0.45	0.52	0.40	0.50	0.41	0.38
Ti_C	0.11	0.10	0.10	0.10	0.11	0.11	0.09	0.13	0.13	0.13	0.11	0.11	0.11	0.13	0.12	0.09	0.11	0.12
Mg_C	3.11	3.18	3.25	3.04	3.24	3.13	2.18	2.20	2.27	2.33	2.28	2.29	2.30	2.34	2.23	2.16	2.32	2.26
Fe^{2+}_C	0.78	0.61	0.66	0.74	0.76	0.89	1.79	1.92	1.81	1.79	1.72	1.75	1.72	1.61	1.85	1.69	1.77	1.82
Mn_C	0.00	0.01	0.00	0.03	0.00	0.00	0.00	0.00	0.00	0.00	0.00	0.00	0.00	0.00	0.00	0.00	0.00	0.00
Fe^{2+}_B	0.02	0.00	0.03	0.00	0.10	0.06	0.16	0.18	0.15	0.13	0.13	0.13	0.15	0.02	0.16	0.04	0.18	0.15
Mn_B	0.02	0.03	0.03	0.00	0.02	0.03	0.03	0.03	0.05	0.05	0.05	0.05	0.05	0.05	0.05	0.04	0.04	0.03
Ca_B	1.96	1.94	1.94	2.00	1.88	1.91	1.81	1.79	1.80	1.82	1.81	1.82	1.80	1.93	1.79	1.92	1.78	1.82

(*Continued*)

Continued Table 2. Electron-microprobe compositions of hornblende from the Wuhaolai complex

Samples	HC-1	HC-2	HC-3	HC-4	HC-5	HC-6	SC-1	SC-2	SC-3	SC-4	SC-5	SC-6	SC-7	SC-8	SC-9	SC-10	SC-11	SC-12
	gabbro						diorite											
Na_B	0.00	0.03	0.00	0.00	0.00	0.00	0.00	0.00	0.00	0.00	0.00	0.00	0.00	0.00	0.00	0.00	0.00	0.00
Ca_A	0.01	0.00	0.03	0.00	0.03	0.03	0.12	0.10	0.10	0.09	0.09	0.09	0.08	0.03	0.11	0.05	0.14	0.10
Na_A	0.32	0.28	0.29	0.32	0.36	0.36	0.35	0.42	0.38	0.40	0.36	0.37	0.37	0.34	0.38	0.35	0.35	0.39
K_A	0.09	0.08	0.08	0.08	0.08	0.11	0.10	0.12	0.11	0.11	0.11	0.11	0.11	0.11	0.11	0.11	0.10	0.13

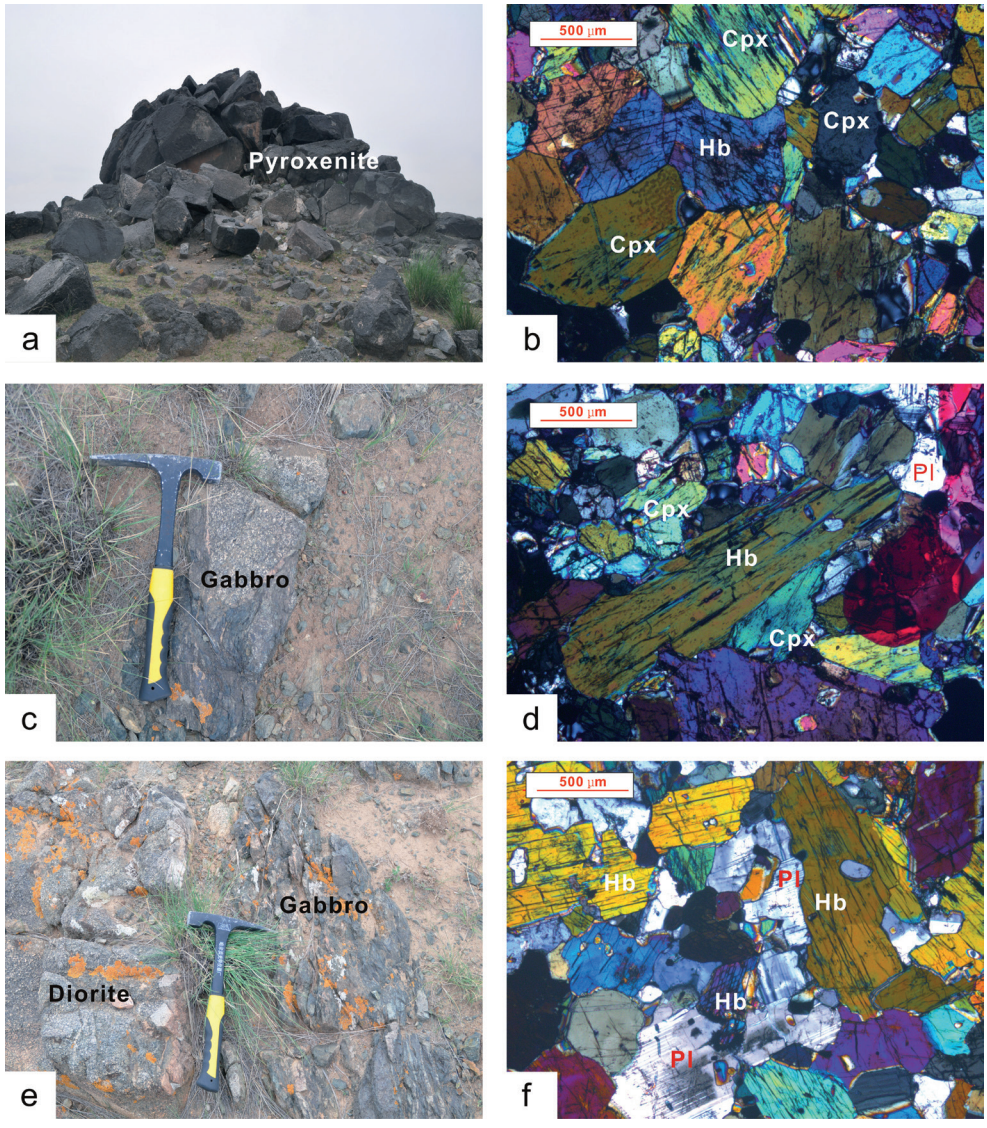

Figure 3. Selected outcrop photographs and microphotographs of the representative rocks from the Wuhaolai complex. (a) field photo of pyroxenite from the Wuhaolao complex; (b) microphotograph of pyroxenite from the Wuhaolao complex (under the cross-polarized light); (c) field photo of gabbro from the Wuhaolao complex; (d) microphotograph of gabbro from the Wuhaolao complex (under the cross-polarized light); (e) lithofacies lines between gabbro and diorite of the Wuhaolao complex; (f) microphotograph of diorite from the Wuhaolao complex (under the cross-polarized light)
Pl: plagioclase, Cpx: clinopyroxene, Hb: hornblende (Whitney and Evans (2010).

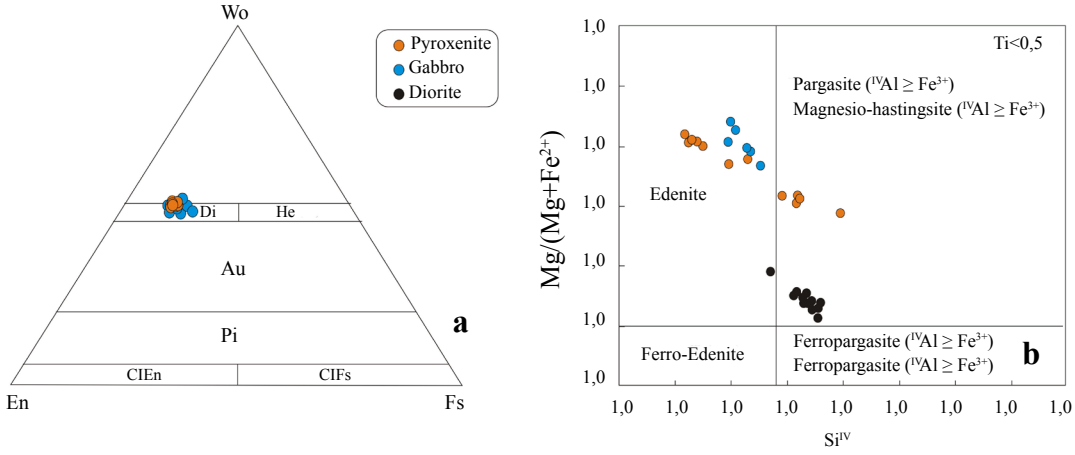

Figure 4. (a) Wo–En–Fs diagram of clinopyroxene in Wuhaolai mafic complex (after Morimoto et al., 1988); (b) Classification of hornblende in the Wuhaolai mafic complex (after Leake et al., 1997). Di: diopside, He: hedenbergite, Au: augite, Pi: pigeonite, En: enstatite/clinoenstatte, C1En: bronzite, C1Fs: ferrohypersthene, Fs: ferrosilite/clinoferrosilite.

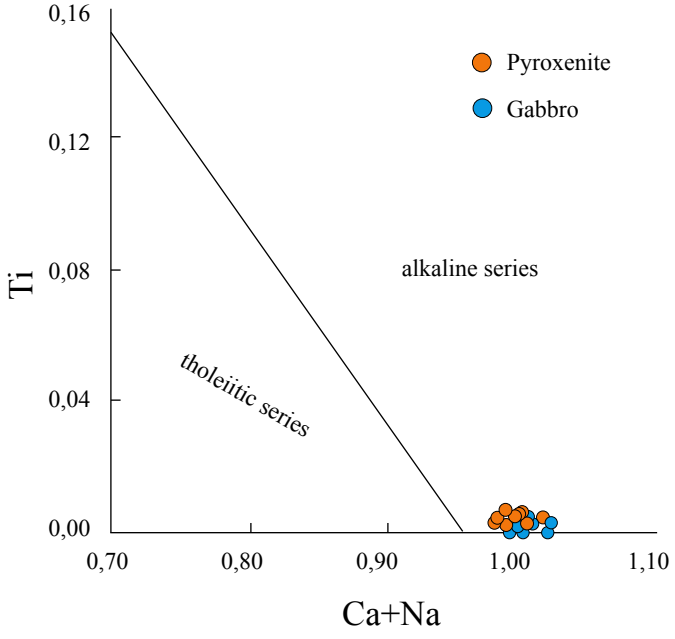

Figure 5. Ti–Ca + Na diagrams for clinopyroxenes (after Leterrier et al., 1982)

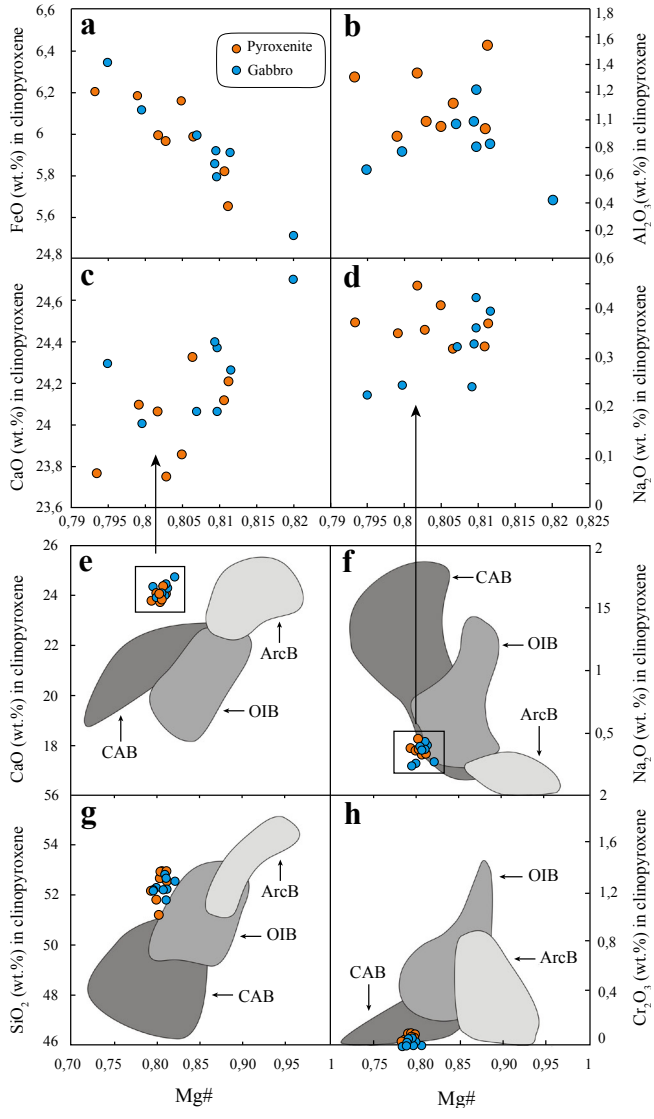

Figure 6. Oxide compound correlation diagrams of clinopyroxene (after Kim et al., 2016), arc basalts (after Debari et al., 1987; Bryant et al., 2007), oceanic island basalts (after Bohrson et al., 1988; Chen et al., 1992; Fodor et al., 1997), and continental alkaline basalts (after Arai et al., 2001; Ho et al., 2000; Kovács et al., 2004).

that the equilibrium state between clinopyroxene and its host rocks can be reflected by the Fe–Mg exchange partition coefficient Kd_{cpx} = $(Fe/Mg)^{Cpx}$ /$(Fe/Mg)^{liquid}$ (Putirka, 1999; Toplis et al, 1995). In this research, the Kd_{cpx} values, which were calculated based on the results of clinopyroxene and whole-rock geochemical (Liu et al., 2017), were between 0.23 and 0.27. Thus, based on Kd_{cpx} and the Mg# of the Wuhaolai clinopyroxenes (77.7–80.6), the Mg# of the equilibrium melt was found to be in the range 43–53 (Fig.8). This relatively low Mg# number indicated that the parental magma may derive from the lithospheric mantle and could have experienced crystal fractionation..

In the Al_2O_3–TiO_2 diagram (Fig. 9a), almost all the hornblende grains from the Wuhaolai complex are consistent with the composition of hornblende from mantle source (Jiang et al., 1984). In addition, the Al/Si values of hornblende from pyroxenite, gabbro and diorite are 0.15–0.30, 0.20–0.21, 0.23–0.28, respectively, and their Mg/(Fe^{3+} + Fe^{2+} + Al^{VI}) values are 1.28–1.96, 1.68–1.92, and 0.75–0.92, respectively, indicating that hornblende compositions are consistent with those from the intermediate–basic magmatic origin (Fig. 9b). All the above features support that hornblende from the Wuhaolai complex is of magmatic origin and not a product of hydrothermal alteration. Additionally, in the Al^{IV}–A, A^{IV}–total Al, and Al^{IV}–Al^{VI} + Fe^{3+} + 2Ti + A sites and in the

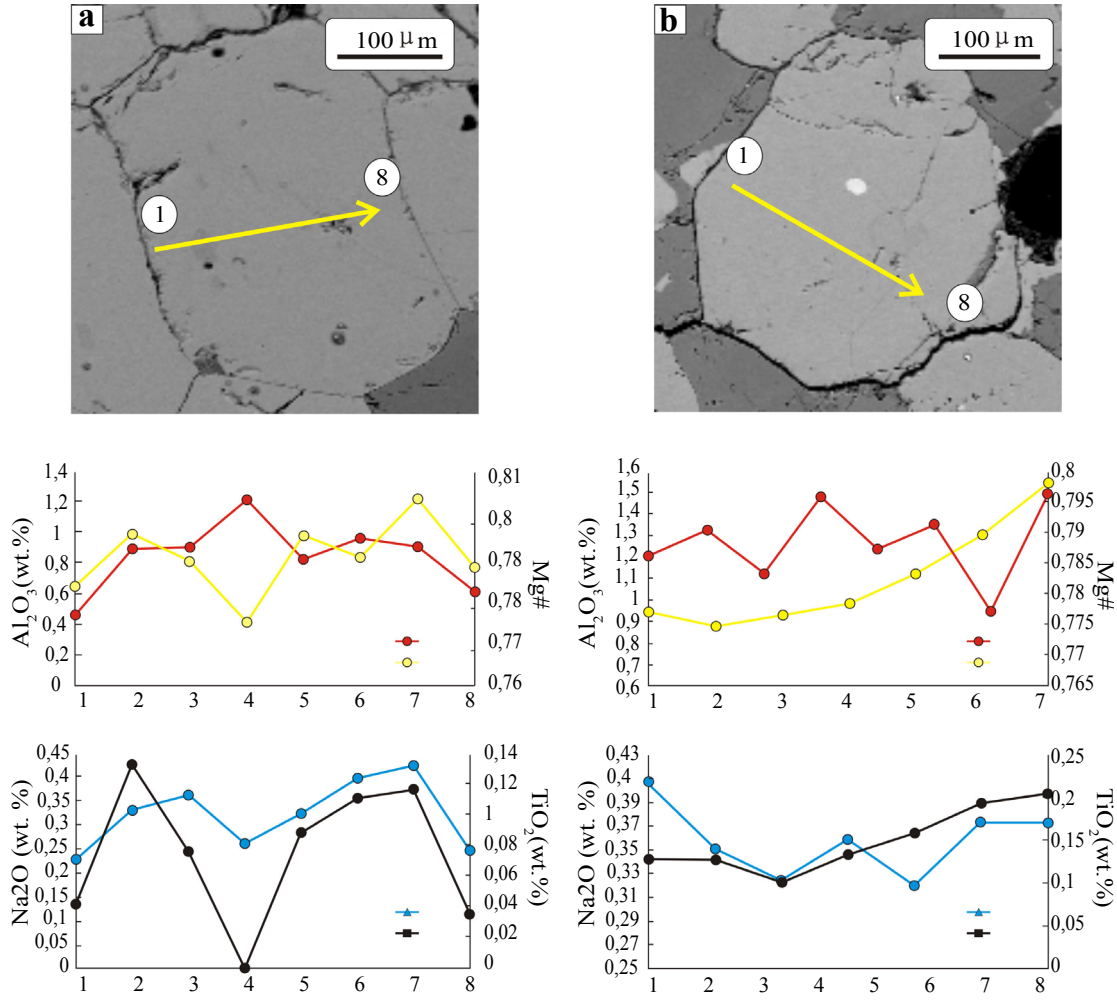

Figure 7. Backscattered electronic images of clinopyroxene crystals from representative samples of the Wuhaolai mafic complex and their compositional profiles. (a) Pyroxenite sample; (b) Gabbro sample.

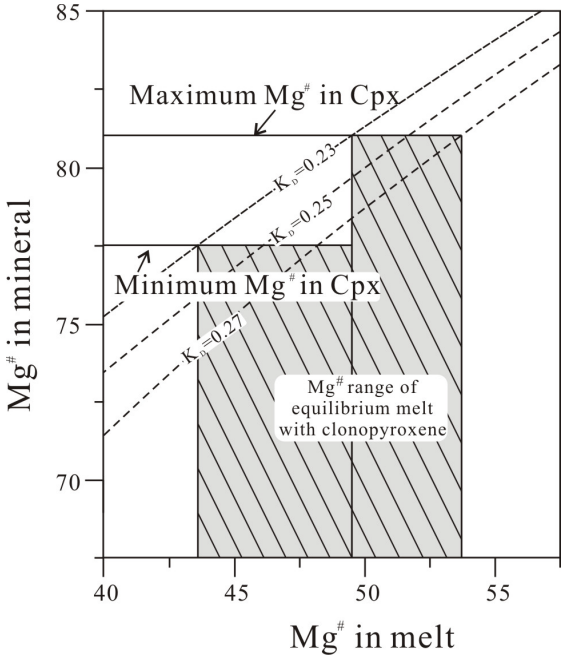

Figure 8. Mineral–melt Fe/Mg equilibrium diagram for clinopyroxene (after Kim et al., 2016).

Al^{IV}–Ti diagrams (Fig. 10), the hornblende compositions in the different rock types exhibit a high linear correlation. This suggests that the electric charge imbalance, which is caused by the four-coordinated Al^{IV}-substitution of Si in the tetrahedral position, may be compensated by the isomorphism replacement of Al^{IV}, Fe^{3+},and Ti in the octahedral position (Niu et al., 2005). Hornblende in peridotite xenoliths can be divided into two types: S-hl and I-hl. S-hl, which originates from the mantle wedge above the subduction zone, is mainly affected by fluids or melts derived from the subducted slab, whereas I-hl, which is formed in the intra-plate environment, is mainly influenced by the metasomatism of asthenospheric materials (I-Amph) (Coltorti et al., 2007). In the SiO_2 vs. Na_2O and SiO_2 vs. TiO_2 diagrams (Fig.11), the analyzed hornblende grains plot into the S-Amph area (Fig. 11), indicating that the magma source may have been modified by the fluids or melts derived from the subducted slab (Xu et al., 2009).

Estimation of mineral crystallization temperature and pressure

Although many clinopyroxene geothermometers have been proposed (Davis et al., 1966; Nimis 1995; Nimis et al., 1999; Putirka et al., 2003), herein, we used the clinopyroxene–liquid geothermometer (Putirka et al. 2003) to estimate the crystallization conditions (temperature and pressure) of clinopyroxene in the Wuhaolai complex. The principle of this method is that the jadeite (Jd; $NaAlSi_2O_6$) content in clinopyroxene is sensitive to the pressure and temperature in the pyroxene–melt exchange reaction (Putirka et al., 2003). Before calculating the crystallization temperature and the pressure,

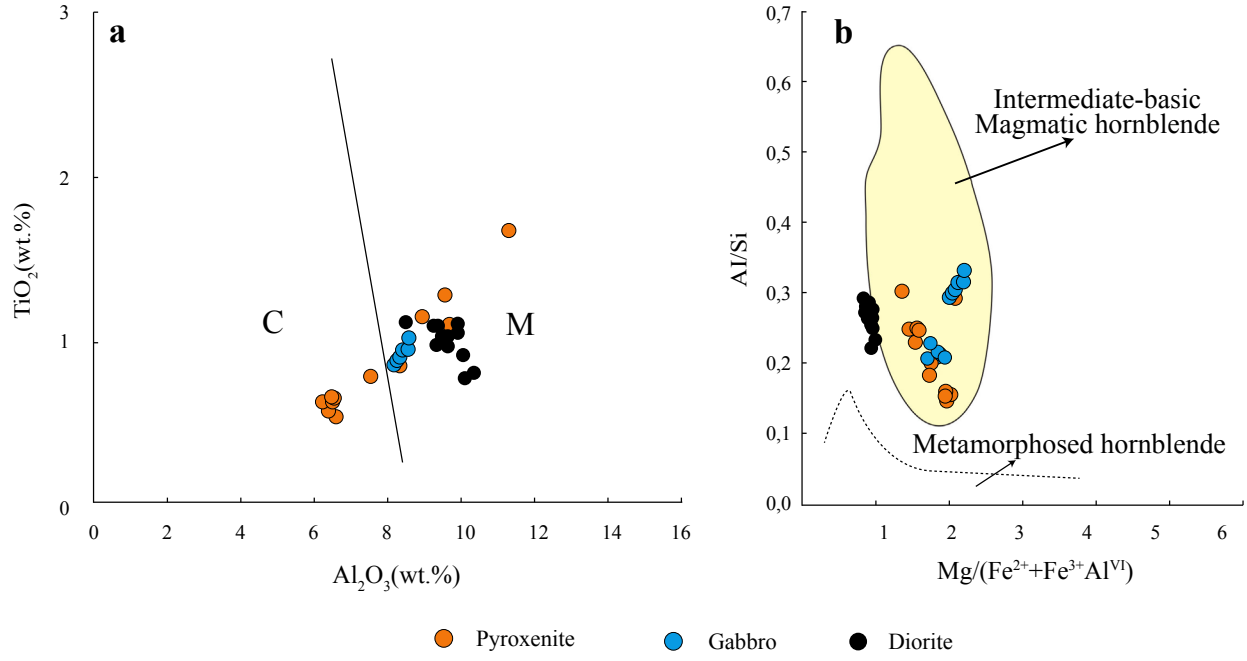

Figure 9. (a) Al_2O_3–TiO_2 diagram for hornblende compositions (after Jiang et al., 1984); (b) Mg/(Fe^{3+} + Fe^{2+} + Al^{VI})–Al/Si diagram of hornblende (after Xue et al., 1986). C: crustal source, M: mantle source.

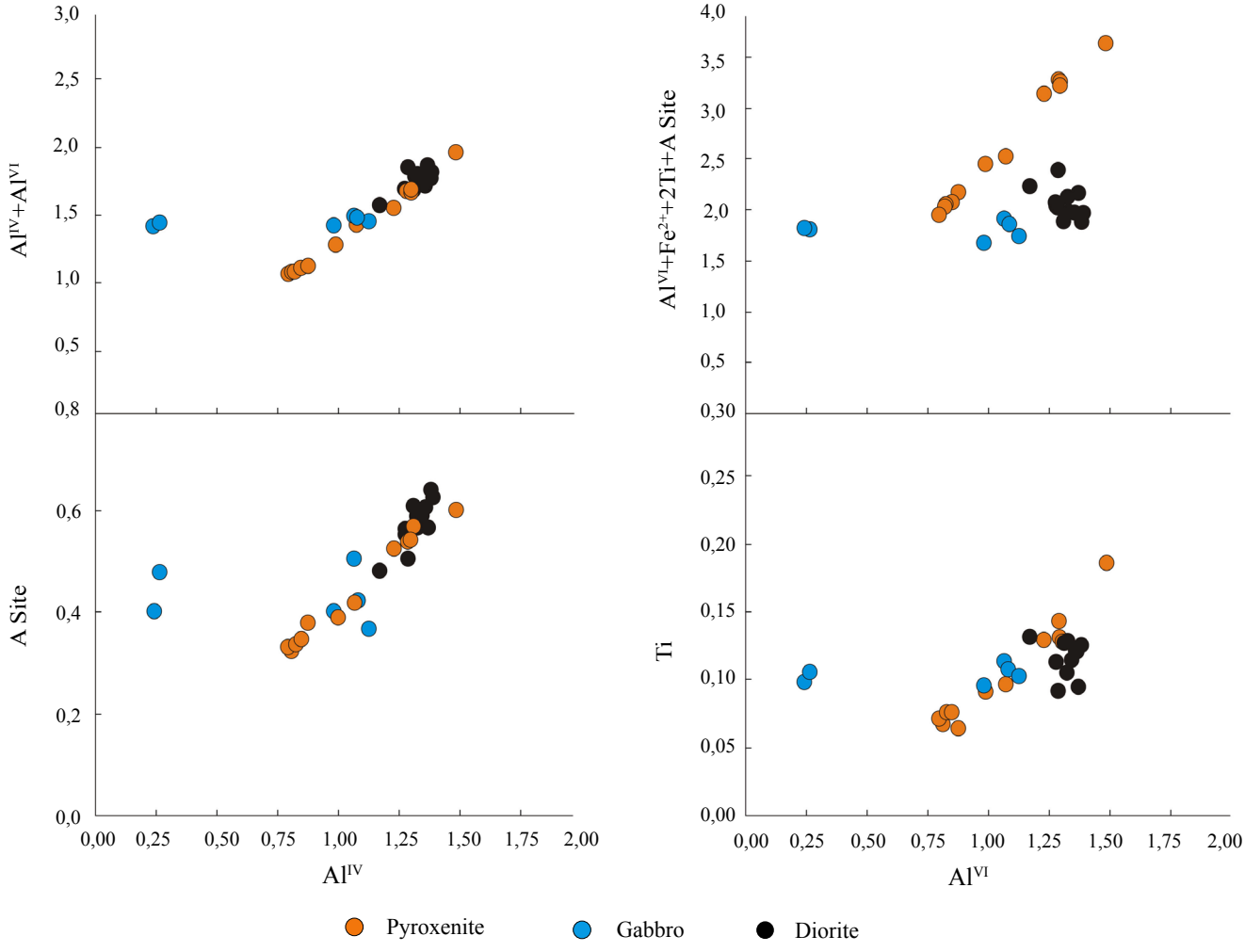

Figure 10. Hornblende compositional variation diagrams.

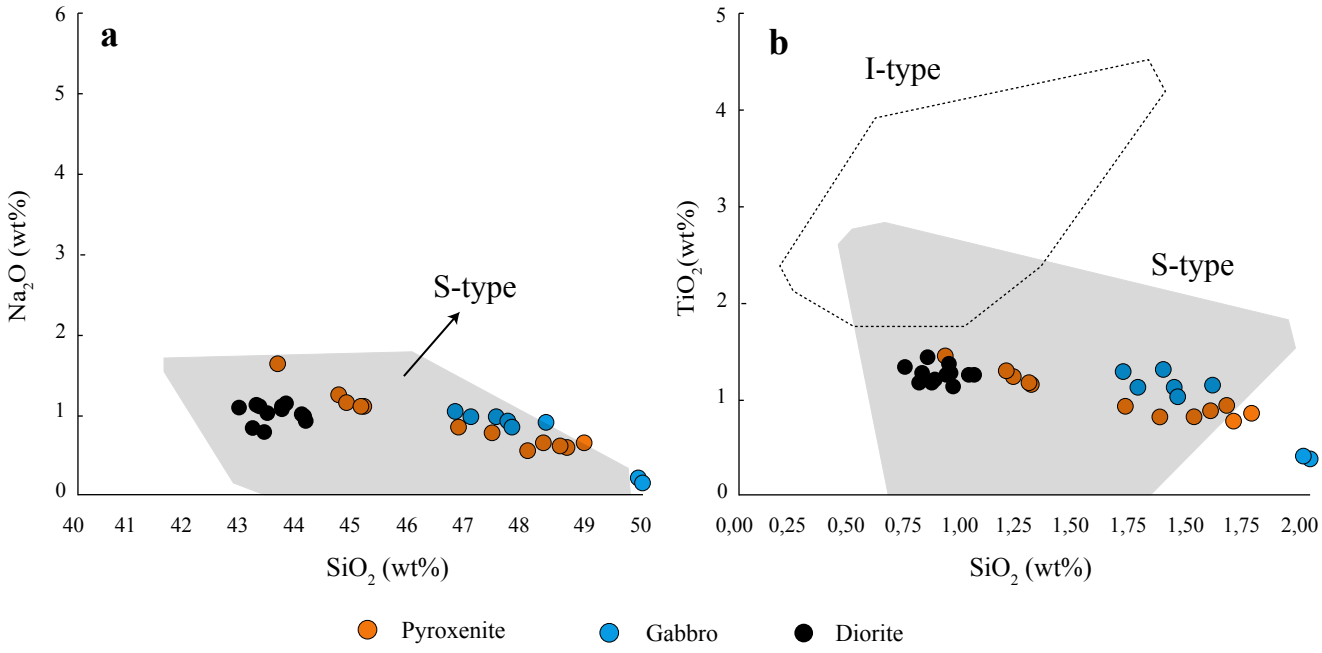

Figure 11. SiO_2 versus Na_2O and TiO_2 diagrams for hornblende (after Coltorti et al., 2007).

we should verify whether clinopyroxene and its host rocks have reached an equilibrium state (chen et al., 2015). Experimental results indicated that when clinopyroxene and its host rocks reached the equilibrium state, the Kd_{cpx} values were between 0.2 and 0.4 (Irving et al., 1984; Liotard et al., 1988; Kinzler et al., 1997; Hunter et al., 1997). In this research, the Kd_{cpx} values are in the range 0.23–0.27, indicating that clinopyroxene and the melt have reached the equilibrium state. This is also supported by the normal zonal texture of clinopyroxene. Thus, based on the study conducted by Putirka et al. (2003), the crystallization temperature of clinopyroxene in pyroxenite ranged from 1426°C to1434°C and the crystallization pressure ranged from 1.1 to 1.7 GPa. The crystallization temperature of clinopyroxene in gabbro was 1382°C–1389°C, whereas the crystallization pressure was in the range 0.5–1.3 GPa. Therefore, the crystallization temperature and pressure for pyroxenite were slightly higher than those for gabbro, suggesting that the formation depth of gabbro was slightly shallower than the pyroxenite.

Tectonic significance

Due to the subduction of the PAO, various types of late Paleozoic plutons were widely distributed in the northern margin of the NCC. However, Wulan granodiorites (323.4 ± 3.4 Ma) (Zhang et al., 2011), Wengeng gabbro (280 Ma) (Zhao et al., 2008), Shihahe biotite monzonitic granite (275.0 ± 0.7 Ma) (Hao et al., 2016), and Ondor Sum–Tieshagai intermediate–felsic intrusions (271 ± 2.4 Ma) (Wang et al., 2013) were formed under an active continental margin tectonic setting. The Kebu pluton (291 ± 4 Ma) (Luo et al., 2007), the Beiqigetao mafic pluton (269 ± 8 Ma) (Zhao et al., 2011), and the Tugurige hornblendite (273.5 ± 1.3 Ma) (Wang et al., 2016) exhibited the characteristics of the post-collisional extension environment. Thus, the PAO finally closed at the early–middle Permian. This was further supported by the paleontological results of the Cathaysian flora of the early–middle Permian stratum in the southern margin of the Siberian plate (Zhou et al., 2010). Besides, in the TiO_2–MnO–Na_2O diagram of Nisbet et al. (1977) (Fig. 12), clinopyroxenes from pyroxenite and gabbro of the Wuhaolai mafic complex mainly belong to the within-plate alkali basalt (WPA) field. Therefore, combining the geochemical characteristics of the unpublished zircon U–Pb data (265 Ma), the Wuhaolai complex was formed in the within-plate tectonic setting in the middle Permian. Combining all these results with the chemical characteristics of the studied clinopyroxene and hornblende crystals in pyroxenite and gabbro samples from the Wuhaolai

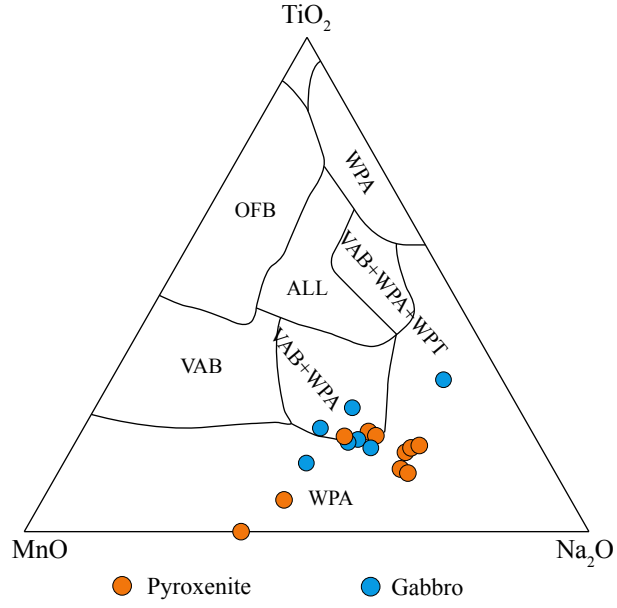

Figure 12. TiO_2–MnO–Na_2O diagram for clinopyroxene composition of pyroxenite and gabbro samples from the Wuhaolai mafic complex (after Nisbet et al., 1977).
WPT: within-plate tholeiitic; WPA: within-plate alkali basalt; VAB: volcanic arc basalt; OFB: ocean floor basalt.

mafic complex, it can be drawn that the magma source of this complex was modified by fluids or melts derived from the subducted slab in the course of the PAO subduction under the northern NCC margin (Zhao et al., 2011; Tang et al., 2014., Wang et al., 2016). Therefore, it can be conjectured that the parental magma of the Wuhaolai complex may derived from partial melting of an enriched lithospheric mantle source after the PAO closure (Zhao et al., 2011, Hou et al., 2014, Zhang et al., 2011). The clinopyroxene and the hornblende in the studied rocks were produced along with the fractional crystallization of the parental magma of the Wuhaolai complex.

Conclusions

The conclusions of our study are summarized as follows:

1. The parental magma of the Wuhaolai mafic complex belongs to the intra-plate alkaline series. The feature of the normal chemical zoning and the other chemical characteristics documented for clinopyroxene in the studied samples of pyroxenite and gabbro from the Wuhaolai mafic complex are attributed to the crystallization process of the same parental magma. Additionally, the chemical characteristics of hornblende (S-hl) in the studied samples suggest that the magma source may have been modified by the fluid or melt derived from the subducted slab.
2. The Fe–Mg exchange partition coefficient Kd_{cpx} calculated for the Wuhaolai mafic complex range from 0.23 to 0.27. Furthermore, the crystallization temperature and pressure calculated for the gabbro unit are lower than those of pyroxenite, suggesting that the formation depth of gabbro was slightly shallower than that of pyroxenite.
3. Based on the characteristics of the rock-forming minerals, the Wuhaolai mafic complex is interpreted as formed in a within-plate tectonic setting, where clinopyroxene with normal zoning feature and hornblende were crystallized resembling some chemical imprints related with subduction fluids.

Acknowledgements

We appreciate K.Y. Bai, M.W. Liu, L.L. Xu, and X.J. Tan for providing support during the investigation conducted using electron microprobes. We are also grateful to the anonymous reviewers and editors for their meaningful and valuable comments that greatly improved the manuscript. This work was supported by Geological investigation work project of China Geological Survey (12120115069701) and Fundamental Research Funds for the Central Universities (No. 300102278402).

References

Arai, S., Abe, N., & Hirai, H. (2001). Geological, petrographical and petrological characteristics of ultramafic-mafic xenoliths in Kurose and Takashima, northern Kyushu, southwestern Japan. *Science Reports of Kanazawa University,* 46(01-02), 9–38.

Bohrson, W. A., & Clague, D. A. (1988). Origin of ultramafic xenoliths containing exsolved pyroxenes from Hualalai volcano, Hawaii. *Contributions to Mineralogy and Petrology*, 100(02), 139–155.

Bowen, N. L. (1928). *The Evolution of The Igneous Rocks*. Princeton University Press, 332.

Bryant, J. A., Yogodzinski, G. M., & Churikovca, T. G. (2007). Melt–mantle interactions beneath the Kamchatka arc: evidence from ultramafic xenoliths from Shiveluch volcano. *Geochemistry, Geophysics, Geosystems,* 8(4), Q04007.

Cao, S. R., Guo, X. A., & Wu, Z. L. (2002). Geology of the Inner Mongolia Autonomous Region (Ma, L.F., Qiao, X.F., Min, R.L. Geological Atlas of China). Beijing: Geological Publishing house, 1–348 (in Chinese with English abstract).

Chen, C. H., Presnall, D. C., & Stern, R. J. (1992). Petrogenesis of ultramafic xenoliths from the 1800 Kaupulehu flow, Hualalai volcano, Hawaii. *Journal of Petrology*, 33(1), 163–202.

Chen, Z. Q., Jiang, S. Y., Xu, Y. M., Zhu, Z. Y., & Zhou, W. (2015). Petrogenesis and magma evolution of Tertiary basalts from the Langjunshan area in the Jiurui mineralization district, Jiangxi Province: Evidence from pyroxene and feldspar (in Chinese with English abstract). *ActaPetrologica Sinica*, 31(3), 686-700.

Coltorti, M., Bonadiman, C., Faccini, B., Gregoir, M., O'Reilly, S.Y., & Powell, W. (2007). Amphiboles from suprasubduction and intraplate lithospheric mantle. *Lithos,* 99(1-2),68–84.

Condie, K.C. (1982). *Plate Tectonics and Crust Evolution*. New York: Pergamon Press.

Davis, G. A., Zheng, Y. D., & Wang, C. (2001). *Mesozoic tectonic evolution of the Yanshan fold and thrust belt, with emphasis on Hebei and Liaoning Provinces, Northern China*. In: Hendrix, M. S., & Davis, G. A. (Eds.) Paleozoic and Mesozoic tectonic evolution of central Asia: From continental assembly to intracontinental deformation. Geological Society of America Memoir, 194: 171–197.

Debari, S., Kay, S. M., & Kay, R. W. (1987). Ultramafic xenoliths from Adagdak volcano, Adak, Aleutian Islands, Alaska: deformed igneous cumulates from the Moho of an island arc. *Journal of Geology*, 95(3), 329–341.

Dobosi, G., & Fodor, R. V. (1992). Magma fractionation, replenishment, and mixing as inferred from green-core clinopyroxenes in Pliocene basanite, southern Slovakia. *Lithos,* 28(2), 133–150.

Fodor, R. V., & Galar, P. (1997). A view into the subsurface of Mauna Kea Volcano, Hawaii: crystallization processes interpreted through the petrology and petrography of gabbroic and ultramafic xenoliths. *Journal of Petrology,* 38(5), 581–624.

Han, B. F, Wang, S. G., Jahn, B. M., Hong, D. W., Kagamid, H., & Suna, Y. L. (1997). Depleted mantle source for the Ulungur River A-type granites from North Xinjiang, China: geochemistry and Nd–Sr isotopic evidence, and implications for the Phanerozoic crustal growth. *Chemical Geology,* 138(3-4), 135–159.

Haase, K. M., Hartmann, M., & Wallrabe-Adams, H. J. (1996). The geochemistry of ashes from Vesterisbanken Seamount, Greenland Basin: implications for the evolution of an alkaline volcano. *Journal of Volcanology and Geothermal Research,* 70(1-2), 1–19.

Hao, Z. Y., Niu, Y. F., Chen, M. C., Gao, Y., Chen, H. D., & Niu, X. N. (2016). LA-ICP-MS zircon U-Pb dating of the biotite monzonitic granite from Shihahe area in Inner Mongolia and its geological significance (in Chinese with English abstract). *Geology In China,* 43(1), 72–80.

Ho, K., Chen, J., Smith, A. D., & Juang, W. S. (2000). Petrogenesis of two groups of pyroxenite from Tungchihsu Penghu Islands, Taiwan Strait: implications for mantle metasomatism beneath SE China. *Chemical Geology*, 167(3-4), 355–372.

Hou, J. G., Su, S. G., Zhou, D., & Wang, Q. (2014). Petrological and geochemical characteristics of basic-ultrabasic complex from southern Wengen in Inner Mongolia and its tectonic setting (in Chinese with English abstract). *Acta Petrologica Sinica,* 30(12), 3729–3740.

Jian, P., Liu, D. Y., Kröner, A., Windley, B. F., Shi, Y. R., Zhang, W., Zhang, F. Q., Miao, L. C., Zhang, L. Q.,, & Tomurhuu, D. (2010). Evolution of a Permian intraoceanic arc-trench system in the Solonker suture zone, Central Asian Orogenic Belt, China and Mongolia. *Lithos,* 118(1-2), 169–190.

Jiang, C. Y., & An, S. Y. (1984). On Chemical Characteristics of Calcic Amphiboles from Igneous Rocks and Their Petrogenesis Significance (in Chinese with English abstract). *Acta Mineralogy Sinica*, 03, 1–9.

Kheraskova, T. N.,Volozh, Y. A., Didenko, A. N., & Bush, V. A. (2003). The Vendian-Early Paleozoic history of the continental margin of Eastern Paleogondwana, Paleoasian Ocean, and Central Asian Foldbelt. *Russian Journal of Earth Sciences*, 5(3), 165–184.

Kovács, I., Zajacz, Z., & Szabó, C. (2004). Type-II xenoliths and related metasomatism from the Nógrád-Gömör Volcanic Field, Carpathian-Pannonian region (northern Hungry-southern Slovakia). *Tectonophysics,* 393(1-4), 139–161.

Kusky, T. M., Windley, B. F., & Zhai, M. G. (2007). Tectonic evolution of the North China Block: from orogen to craton to orogen. *Geological Society London Special Publications*, 280(1), 1–34.

Leake, B. E., Woolley A. R., Arps, C. E. S., Birch, W. D., Gilbert, M. C..., & Guo, Y. Z. (1997). Nomenclature of amphiboles: Report of the Subcommittee on Amphiboles of the International Mineralogical Association, Commission on New Minerals and Mineral Names. *International Conference on Formal Concept Analysis*, 4390(7), 181-196.

Leterrier, J., Maury, R. C., & Thonon, P. (1982). Clinopyroxene composition as a method of identification of the magmatic affinities of paleo-volcanic series. *Earth and Planetary Science Letters*, 59, 139-154

Liu, J., Wang, C., Liu, Y., Zhang, H., Ge, J. (2017). Middle Permian Wuhaolai mafic complex in the northern North China Craton: Constraints on the subduction‐related metasomatic mantle and tectonic implication. *Geological Journal,* 1–19. DOI: https://doi.org/10.1002/gj.3085

Li, J.Y. (2006). Permian geodynamic setting of Northeast China and adjacent regions: closure of the Paleo-Asian Ocean and subduction of the Paleo-Pacific Plate. *Journal of Asian Earth Science*, 26(3-4), 207–224.

Li, Y. L., Zhou, H. W., & Brouwer. (2014a). Nature and timing of the Solonker suture of the Central Asian Orogenic Belt: insights from geochronology and geochemistry of basic intrusions in the Xilin Gol Complex, Inner Mongolia, China. *Internal Journal of Earth Sciences*, 103(1), 41–60.

Li, Y. L., Zhou, H. W., Brouwer, F. M., Xiao, W. J., Wijbrans, J. R., & Zhong, Z. Q. (2014b). Early Paleozoic to Middle Triassic bivergent accretion in the Central Asian Orogenic Belt: insights from zircon U–Pb dating of ductile shear zones in central Inner Mongolia, China. *Lithos,* 205(9), 84–111.

Liu, Y. R., Lv, X. B., Mei, W., & Dai, Y. C. (2012). Mineralogy of clinopyroxene from Pobei mafic-ultramafic complex in Beishan area , Xinjiang , and its geological significance (in Chinese with English abstract). *Acta Petrologica ET Mineralogica*, 31(2), 212-224.

Lu, Y. F. (2004). GeoKit - A geochemical toolkit for Microsoft Excel (in Chinese with English abstract). *Geochimica,* 33(05), 459-464.

Inner Mongolia Bureau of Geology and Mineral Resources (1991). *Regional geology of the Inner Mongolia Autonomous Region* (in Chinese with English abstract). Beijing: Geological Publishing House.

Luo, H. L., Wu, T. R., & Li, Y. (2007). Geochemistry and SHRIMP dating of the Kebu massif from Wulatezhongqi, Inner Mongolia: evidence for the Early Permian underplating beneath the North China Craton (in Chinese with English abstract). *Acta Petrologica Sinica,* 23(4), 755–766.

Menzies, M. A., Fan, W., & Zhang, M. (1993). Palaeozoic and Cenozoic lithoprobes and the loss of >120 km of Archean lithosphere, Sino-Korean craton, China. *Geological Society of London Special Publications*, 76(1), 71–81.

Morimoto, N. (1988). Nomenclature of pyroxenes. *Acta Mineralogica*, 8(4), 289–305.

Kim, N. Y., & Choi, S. N. (2016). Petrogenesis of Late Triassic ultramafic rocks from the Andong Ultramafic Complex, South Korea. *Lithos,* 264(1), 28-40.

Nisbet, E. G., & Pearce, J. A. (1977). Clinopyroxene composition in maficlavas from different tectonic settings. *Contributions to Mineralogy and Petrology*, 63(2), 149–160.

Niu, L. F., & Zhang, H. F. (2005). Mineralogy and petrogenesis of amphiboles from intermediate - mafic intrusions in southern Taihang Mountains (in Chinese with English abstract). *Geotectonica Et Metallogenia*, 29(2), 269–277.

Pan, Y. Q. (1996). Early Permian Bajiazi Ultra-Unit Intrusive Rock from and its Emplacement Mechanism Jianping Area. *Liaoning Geology*, 04, 284–292.

Putirka, K. (1999). Clinopyroxene + liquid equilibria to 100 kbar and 2450 K. *Contributions to Mineralogy and Petrology,* 135(2-3), 151–163.

Robinson, P. T., Zhou M. F., Hu X. F., Reynolds, P., Bai, W. J., &Yang, J. S. (1999). Geochemical constraints on the origin of the Hegenshan ophiolite, Inner Mongolia, China. *Journal of Asian Earth Science*, 17(4), 423–442.

Shi, G. Z., Faure, M., Xu, B., Zhao, P., & Chen, Y. (2013). Structural and kinematic analysis of the Early Paleozoic Ondor Sum-Hongqi mélange belt, eastern part of the Altaids (CAOB) in Inner Mongolia, China. *Journal of Asian Earth Sciences*, 66(5), 123–139.

Su, B. X., Qin, K. Z., Sun, H, Tang, D. M., Xiao, Q. H.,&Cao, M. J. (2009). Petrological and mineralogical characteristics of Hongshisha mafic-ultramafic complex in Beishan area, Xinjiang: Implications for assimilation and fractional crystallization (in Chinese with English abstract). Acta Petrologica Sinica, 25(4), 873–887.

Su, B. X., Qin, K. Z., Sun, H, Tang, D .M., Xiao, Q. H.,& Cao, M.J. (2009). Petrological and mineralogical characteristics of Hongshisha mafic-ultramafic complex in Beishan area, Xinjiang: Implications for assimilation and fractional crystallization (in Chinese with English abstract. *Acta Geologica Sinica*, 82(11), 1602–1612).

Tang, Y. J., Zhang, H. F., & Ying, J. F. (2014). Genetic significance of Triassic alkali-rich intrusive rocks in the Yinshan and neighboring areas (in Chinese with English abstract). *Acta Petrologica Sinica*, 30(7), 2031–2040.

Toplis, M. J., & Carroll, M. R. (1995). An experimental study of the influence of oxygen fugacity on Fe–Ti oxide stability, phase relations, and mineral-melt equilibria in ferro-basaltic systems. *Journal of Petrology*, 36(5), 1137–1170.

Xiao, W. J., Windley, B. F., Hao, J., & Zhai, M. G. (2003). Accretion leading to collision and the Permian Solonker suture, Inner Mongolia, China: termination of the central Asian orogenic belt. *Tectonics*, 22(6), 1484-1505.

Wang, J., Sun, F. Y., Li, B. L., Wang, Y. D., & Li, R. H. (2016). Age Petrogenesis and Tectonic Implications of Permian Hornblendite in Tugurige, Urad Zhongqi, Inner Mongolia (in Chinese with English abstract). *Earth Science*, 41(5), 792–808.

Wang, W. Q., Xu, Z. Y., Liu, Z. H., Zhao, Q. Y., & Jiang, X. J. (2013). Early-Middle Permian tectonic evolution of the central-northernmargin of the North China Craton: Constraints from zircon U-Pb ages and geochemistry of the granitoids (in Chinese with English abstract). *Acta Petrologica Sinica*, 29(9), 2987–3003.

Whitney, D. L. & Evans, B. W. (2010) Abbreviations for names of rock-forming minerals. *American Mineralogist* 95: 185-187. DOI: 10.2138/am.2010.3371.

Wilde, S. A., Zhao, G. C., & Sun, M. (2002). Development of the North China craton during the Late Archaean and its final amalgamation at 1.8 Ga; some speculations on its position within a global Palaeoproterozoic supercontinent. *Gondwana Research*, 5(1), 85–94.

Wilde, S. A., Zhou, X. H., Nemchin, A. A.,& Sun, M. (2003). Mesozoic crust–mantle interaction beneath the North China craton: a consequence of the dispersal of Gondwanaland and accretion of Asia. *Geology,* 31(9), 817–820.

Windley, B. F., Alexeiev, D., Xiao, W. J., & Badarch, G. (2007). Tectonic models for accretion of the Central Asian orogenic belt. *Journal of the Geological Society of London*, 164(12), 31–48.

Wu, F. Y., Xu, Y. G., Gao, S., & Zheng, J. P. (2008). Lithospheric thinning and destruction of the North China Craton (in Chinese with English abstract). *Acta Petrologica Sinica*, 24(6):1145–1174.

Wu, T. R., He, G. Q., & Zhang, C. (1998). On paleozoic tectonic in the Alxa Region, Inner Mongolia, China. *Acta Geologica Sinica,* 72(3), 256–263.

Xu, W. L., Yang, D. B., Pei, F. P., Wang, F., & Wang, W. (2009). Mesozoic Lithospheric Mantle Modified by Delaminated Lower Continental Crust in the North China Craton: Constraints from Compositions of Amphiboles from Peridotite Xenoliths (in Chinese with English abstract). *Journal of Jilin University (Earth Science Edition),* 3(39), 606-617.

Xue, J. Z., Bai, X. L., & Chen, W. (1986). Genetic mineralogy (in Chinese with English abstract). Wuhan: China University of Geosciences press, 114–121.

Yang, J. H., Wu, F. Y., Wilde, S. A., Belousova, E., & Griffin, W. L. (2008). Mesozoic decratonization of the North China Block. *Geology,* 36(6), 467–470.

Ying, J. F., Zhang, H. F., & Tang, Y. J. (2011). Crust-mantle interaction in the central North China Craton during the Mesozoic: evidence from zircon U-Pb chronology, Hf isotope and geochemistry of syenitic-monzonitic intrusions from Shanxi province. *Lithos*, 125(1-2), 449–462.

Yu L. F., Zhao W. X., Chen J. L., Guo, Q., & Wang B. D. (2011). Compositional zone investigation of clinopyroxene phenocryst in the Cenozoic ultra-potassic rocks from the middle-southern Lhasa block. *Acta Petrologica Sinica,* 27(12), 3666–3674.

Zhang, Q. W., Liu, Z. H., Chai, S. L., Xu, Z. Y., Zhao, Q. Y., & Xu, X. C. (2011). Geochronology and Geochemistry of Granodiorites from Wulan Area of Urad Zhongqi, Inner Mongolia (in Chinese with English abstract). *Journal of Mineralogy and Petrology,* 31(2), 7–14.

Zhang, S. H., Zhao, Y., Song, B., Yang, Z. Y., Hu, J. M., & Wu, C. H. (2007a). Carboniferous granitic plutons from the northern margin of the North China block: Implications for a late Paleozoic active continental margin. *Journal of the Geological Society of London*, 164(2), 451–463.

Zhang, S. H., Zhao, Y., Song, B., & Liu, D. Y. (2007b). Petrogenesis of the Middle Devonian Gushan diorite pluton on the northern margin of the North China block and its tectonic implications. *Geological Magazine*, 144(144),16-24.

Zhang, S. H., Zhao, Y., Song, B., Hu, J. M., Liu, S. W., Yang, Y. H., Chen, F. K., Liu, X. M., & Liu, J. (2008). Contrasting Late Carboniferous and Late Permian–Middle Triassic intrusive suites from the northern margin of the North China craton: geochronology, petrogenesis and tectonic implications. *Geological Society America Bulletin,* 121(121), 181-200.

Zhang, X. H., & Zhai, M. G. (2010). Magmatism and its metallogenetic effects during the Paleozoic continental crustal construction in northern North China: An overview (in Chinese with English abstract). *Acta Petrologica Sinica*, 26(5), 1329-1341.

Zhao, G. C., Wilde, S. A., & Cawood, P. A. (2001). Archean blocks and their boundaries in the North China craton: Lithological, geochemical, structural and P-T path constraints and tectonic evolution. *Precambrian Research*, 107(1-2), 45–73.

Zhao, L. (2008). *Geochemistry and Tectonic Implications of the Late Palaeozoic mafic-ultramafic rocks belt on the middle segment of the northern margin of the North China Plate.* Peking University.

Zhao, L., Wu, T. R., Luo, H. L., & He, Y. K. (2008). Petrology, Geochemistry and Tectonic Implications of the Wengeng Gabbros in Wulatezhongqi Area, Inner Mongolia (in Chinese with English abstract). *Acta Scientiarum Naturalium Universitatis Pekinensis,* 44(2), 201–211.

Zhao, L., Wu, T. R., Luo, H. L., He, Y. K., & Jing, X. (2008). Geochemistry of Huheengeer Complex, Bayan Obo Region, Inner Mongolia and its Tectonic Implications (in Chinese with English abstract). *Geological Journal of China Universities*, 14(01), 29–38.

Zhao, L., Wu, T. R., Luo, & H. L. (2011). SHRIMP U-Pb dating, geochemistry and tectonic implications of the Beiqigetao gabbros in Urad Zhongqi area, Inner Mongolia (in Chinese with English abstract). *Acta Petrologica Sinica*, 27(10), 3071–3082.

Zhao, P., Chen, Y., & Xu, B. (2013). Did the Paleo-Asian Ocean between North China Block and Mongolia Block exist during the late Paleozoic? First paleomagnetic evidence from central-eastern Inner Mongolia. Journal of Geophysical Research-solid Earth, 118(5), 1873-1894.

Zou, J. X., Liu, X. F., Deng, J. H., Ren, K. F., Li, C. H., Huang, Y. P., ..., & Yi, L. W. (2013). Research of the Clinopyroxene Zoning Phenomenon from the Basic-Ultrabasic Rocks in Jiulong Area, Shangri-La County, Yunnan Province, China (in Chinese with English abstract). *Acta Mineralogy Sinica,* 33(2), 210–220.